SIAM J. Appl. Math.
Vol. 70, No. 7, pp. 2390–2408

DYNAMICS OF THREE-DIMENSIONAL GRAVITY-CAPILLARY SOLITARY WAVES IN DEEP WATER*

BENJAMIN AKERS† AND PAUL A. MILEWSKI‡

Abstract. A model equation for gravity-capillary waves in deep water is proposed. This model is a quadratic approximation of the deep water potential flow equations and has wavepacket-type solitary wave solutions. The model equation supports line solitary waves which are spatially localized in the direction of propagation and constant in the transverse direction, and lump solitary waves which are spatially localized in both directions. Branches of both line and lump solitary waves are computed via a numerical continuation method. The stability of each type of wave is examined. The transverse instability of line solitary waves is predicted by a similar instability of line solitary waves in the nonlinear Schrödinger equation. The spectral stability of lumps is predicted using the waves' speed energy relation. The role of wave collapse in the stability of these waves is also examined. Numerical time evolution is used to confirm stability predictions and observe dynamics, including instabilities and solitary wave collisions.

Key words. water wave, solitary wave, nonlinear Schrödinger equation, gravity-capillary wave, wave collapse

AMS subject classifications. 76B45, 76B25, 76B15

DOI. 10.1137/090758386

1. Introduction.

Gravity-capillary waves are surface waves in the regime where the restoring effects of both gravity and surface tension are similar in magnitude. For an air-water interface, this implies a free-surface length scale of approximately 1 cm. At this length scale, the phase speed has a minimum about which waves are locally nondispersive. Gravity-capillary solitary waves are localized, traveling, nonlinear waves whose Fourier transform decays rapidly away from this minimum. Unlike the classic shallow water solitary wave, these waves are oscillatory. On a one-dimensional (1D) free surface of a two-dimensional (2D) fluid domain, gravity-capillary solitary waves resemble traveling wavepackets. On a 2D free surface, the waves' cross section in the propagation direction is similar to the 1D solitary waves, but, transverse to the propagation direction, the waves either are constant (for so-called line solitary waves) or decay at infinity (for lump solitary waves). Since the wavelength is set by the physical parameters, the deep water (infinite depth) regime is applicable in water deeper than a few centimeters. In this work we ignore the effects of viscosity and surface dissipation which, at this length scale, ultimately need to be included.

In 1989, Longuet-Higgins provided physical motivation for why gravity-capillary solitary waves should exist [1]. Since then, traveling solitary waves have been computed numerically as solutions to the Euler equations in both two and three space dimensions [2, 3, 4, 5, 6] in both shallow and deep water. The existence of such solutions in Euler's equations has been predicted in approximate models [7] and rigorously

*Received by the editors May 7, 2009; accepted for publication (in revised form) March 23, 2010; published electronically June 9, 2010. This research was supported by National Science Foundation grant DMS-0604635.
http://www.siam.org/journals/siap/70-7/75838.html
†Department of Mathematics, Statistics, and Computer Science, University of Illinois at Chicago, 851 S. Morgan St., Chicago, IL 60607 (akers@math.uic.edu).
‡Department of Mathematics, University of Wisconsin, 480 Lincoln Dr., Madison, WI 53706 (milewski@math.wisc.edu).

shown to exist in 1D [8] and 2D shallow water [9]. Gravity-capillary wave dynamics, such as generation from forcing, stability, and collisions, have been considered in shallow water models in one dimension [10, 11, 12] and two dimensions [13] and using envelope and one-way models in two dimensions [14, 15, 16, 17]. Experimental observations of such waves and related flows can be found in [18] and [19].

However, as we have mentioned, the most physically relevant setting in which to study gravity-capillary waves is deep water for which there are few models: in recent work the authors wrote unidirectional model equations for deep water gravity-capillary waves and studied solitary wave dynamics in one dimension [20] and in a weak 2D setting [14]. For the latter case the equation proposed was

$$\eta_t + 2\eta_x + H\left[\eta - \eta_{xx} - 2\eta_{yy}\right] - \frac{3}{2}\eta\eta_x = 0,$$

where H is the Hilbert transform in x, the direction of propagation, and η is the free-surface displacement in a moving frame. In contrast, this paper focuses on a 2D *isotropic* model for gravity-capillary waves in deep water. The model takes the form

$$\eta_{tt} + \Omega^2\eta + N(\eta, \eta_t) = 0,$$

where Ω^2 is the linear operator that yields the full 2D gravity-capillary dispersion relation in deep water and N is a quadratic nonlinear term. (Note that the scaling of the variables is not the same in the two equations.) This new model is used to study the stability dynamics of solitary waves—which are computationally much more challenging for the full Euler equations. To the best of our knowledge, this is the first paper addressing the dynamics of fully 2D deep water gravity-capillary solitary waves.

The paper is organized as follows. In section 2, we derive the model equation as an approximation of the Euler equations. In section 3, we present the branches of numerically computed solitary waves, with connections to the nonlinear Schrödinger (NLS) equation. In section 4, we consider the stability of the numerically computed solitary waves. In section 5, we present the dynamics of unstable solitary waves and collisions of stable solitary waves. Conclusions and future avenues for research are presented in section 6. The numerical method for computing solitary waves is summarized in Appendix A.

2. Derivation. In this section, a nonlinear equation which approximates weakly nonlinear gravity capillary waves in deep water is derived. The equation is a quadratic truncation to the Euler equations (2.1) for an incompressible, irrotational flow with a free surface under the action of both gravity and surface-tension forces. Denoting the horizontal coordinates by $(x, y) \in R^2$ and the vertical coordinate by z, consider the Euler equations, with free-surface boundary conditions, for the velocity potential $\phi(x, y, z, t)$ and the free-surface displacement given by $z = \eta(x, y, t)$:

$$\Delta\phi + \phi_{zz} = 0, \qquad -\infty < z < \epsilon\eta, \tag{2.1a}$$

$$\phi_z = 0, \qquad z = -\infty, \tag{2.1b}$$

$$\eta_t + \epsilon\nabla\eta\cdot\nabla\phi = \phi_z, \qquad z = \epsilon\eta, \tag{2.1c}$$

$$\phi_t + \epsilon\frac{1}{2}(\nabla\phi)^2 + \epsilon\frac{1}{2}(\phi_z)^2 + \eta + \frac{1}{\epsilon}\nabla\cdot\hat{n} = 0, \qquad z = \epsilon\eta. \tag{2.1d}$$

Equation (2.1a), Laplace's equation for ϕ, reflects conservation of mass for irrotational flows. The remaining equations are boundary conditions: decay for the velocity field

with depth (2.1b), the kinematic boundary condition (2.1c) implying the free boundary is carried with the flow, and Bernoulli's equation (2.1d), a statement of conservation of momentum, with the pressure taken to be zero immediately above the free surface. The jump in pressure across the free surface due to surface-tension effects is reflected in the last term in (2.1d) and is proportional to the surface curvature since $\hat{n}$ is the unit normal to the free surface. These equations have been nondimensionalized using a characteristic wave height a, the length scale $L = \gamma^{1/2} g^{-1/2}$, the time scale $\gamma^{1/4} g^{-3/4}$, and the velocity potential scale $a\gamma^{1/4} g^{1/4}$. The parameter $\epsilon = a/L$ will be assumed to be small. In cgs units, $g = 981\text{cm/sec}^2$, and $\gamma = 73.50\text{cm}^3/\text{sec}^2$ is the surface tension coefficient for an air-water interface [21].

Taylor expanding (2.1d) and (2.1c) about the mean level at $z = 0$ yields boundary conditions at that level, and solving Laplace's equation in the lower half-space eliminates the z-dependence of (2.1):

$$\phi(x, y, t, z) = \mathcal{F}^{-1}\left\{\mathcal{F}\left\{\Phi(x, y, t)\right\} e^{|\mathbf{k}|\mathbf{z}}\right\}.$$

Here $\mathcal{F}$ is the Fourier transform in (x, y) with dual variable $\mathbf{k}$. Clearly $\Phi = \phi(x, y, t, 0)$. Derivatives of ϕ with respect to z at $z = 0$ correspond to multiplication of the Fourier transform of Φ by $|\mathbf{k}|$, denoted by $(-\Delta)^{1/2}$ in physical space. This procedure simplifies (2.1) to a system of two equations acting at the mean level. This system, truncated at cubic order in ϕ and η, is

$$\eta_t - (-\Delta)^{1/2}\Phi + \epsilon\nabla\cdot(\eta\nabla\Phi) + \frac{\epsilon^2}{2}\nabla\cdot(\eta^2\nabla(-\Delta)^{1/2}\Phi) = 0, \tag{2.2a}$$

$$\begin{aligned}\Phi_t + (1-\Delta)\eta + \epsilon\left(\frac{1}{2}(\nabla\Phi)^2 + \frac{1}{2}((-\Delta)^{1/2}\Phi)^2 + \eta(-\Delta)^{1/2}\Phi_t\right)\\ + \frac{\epsilon^2}{2}\left(\nabla\cdot(\nabla\eta)^3 + 2\eta(\nabla\Phi\cdot\nabla(-\Delta)^{1/2}\Phi - \Delta\Phi(-\Delta)^{1/2}\Phi) - \eta^2\Delta\Phi_t\right) = 0.\end{aligned} \tag{2.2b}$$

System (2.2) can be formally rewritten in terms of only Φ or η. Eliminating Φ in favor of η, and truncating at quadratic order, yields

$$\eta_{tt} + \Omega^2\eta + \epsilon N(\eta, \eta_t) = 0 \tag{2.3}$$

with

$$N(\eta, \eta_t) = (-\Delta)^{1/2}\left(\frac{1}{2}(\mathcal{H}\eta_t)^2 + \frac{1}{2}\eta_t^2 - \eta\Omega^2\eta\right) - \nabla\cdot(\eta S\nabla\eta + \eta_t\mathcal{H}\eta_t),$$

$$S = (1-\Delta), \quad \Omega^2 = (1-\Delta)(-\Delta)^{1/2}, \quad \text{and} \quad \mathcal{H} = -\nabla(-\Delta)^{-1/2}.$$

The operator $\mathcal{H}$ is the Hilbert transform in (x, y), with Fourier symbol $\hat{\mathcal{H}} = -i\frac{\mathbf{k}}{|\mathbf{k}|}$. Similar techniques can be used to write quadratic truncations in terms of Φ [22]. We note, however, that there are many possible formally consistent ways to write truncated equations, and that they may have quite different behaviors—much like in shallow water, where a variety of Boussinesq systems exist [23]. This truncation was chosen for its relative simplicity and, as we shall see, for having similar focusing properties to NLS models.

We shall use the quadratic nonlinear model (2.3)—henceforth called the Model—to study localized weakly nonlinear wavepacket solitary waves. This model equation is formally equivalent to the full Euler equations (2.1)—henceforth called Euler—to quadratic order, and thus agrees with the Euler equations for triad interactions. Traditionally, weakly nonlinear wavepackets are studied using the associated NLS equation. (This is true in infinite depth; in finite depth there is a leading order mean flow

contribution leading to a Benney–Roskes–Davey–Stewartson system.) In the small amplitude limit, the solitary wave solutions to the associated NLS equation approximate the envelopes of wavepacket solitary waves in the primitive equation. Since the NLS equation has solitary wave solutions only in the focusing regime (related to the relative signs of its coefficients), it can be used to predict the existence of small amplitude wavepacket solitary waves in primitive model equations. In general, the derivation of the NLS equation involves both quadratic and cubic nonlinear terms in the primitive equation. Thus, the model we present, which is, for simplicity, a quadratic truncation of Euler, will have a corresponding NLS equation with different coefficients than a cubic truncation (which would, by definition, have the same coefficients as Euler). Nevertheless the NLS equation for our model has coefficients of the same sign as that of the NLS equation written for Euler equations. Thus, up to a rescaling, these NLS equations will have identical dynamics.

Although a quadratic truncation of Euler neglects cubic interactions, we believe it includes the more important effects neglected by envelope equations altogether. In the NLS approximation the wave envelope is decoupled from the carrier wave, and therefore the phase of the carrier wave relative to the envelope is arbitrary. This has been shown to be incorrect in Euler. We shall see in our quadratic truncation (as in Euler) that many effects (wave profiles, stability, and collision properties) depend on the phase of the carrier wave. This coupling between phase and envelope has been studied in the simplified context of the 5th order Korteweg–de Vries (KdV) equation both numerically [10] and via a "beyond all orders" asymptotic expansion [24]. The 5th order KdV (and in two dimensions the corresponding Kadomtsev–Petviashvili (KP) equation) are the simplest shallow water models for capillary-gravity waves. The goal of this paper is to study *deep water* 2D capillary-gravity solitary waves in a new model equation which can provide information that is outside the scope of the NLS equation.

3. Solitary waves and the nonlinear Schrödinger equation. The solitary wave solutions to the Model resemble traveling wavepackets. The Fourier transform of these waves is localized near $\mathbf{k} = (k, l) = (1, 0)$, and at small amplitudes there is a clear slowly varying wave envelope. The existence of these waves is predicted by two features of the Model: that it has a phase speed minimum at $\mathbf{k} = (1, 0)$ and that the nonlinearity is of the right type. This nonlinear criterion can be tested by checking that the nonlinear coefficient of the corresponding NLS equation has the correct sign. Linear wavepackets have crests which move at the phase speed $|\mathbf{c_p}| = \frac{\omega}{|\mathbf{k}|}$ and envelopes which move at the group velocity $\mathbf{c_g} = \omega_{\mathbf{k}}(\mathbf{k})$. The phase velocity and group velocity are generally different except, for example, when the dispersion relation is isotropic and the phase speed has an extremum. In this case, both velocities are in the same direction and they have equal magnitude since

$$0 = \left(\frac{\omega(|\mathbf{k}|)}{|\mathbf{k}|}\right)' = \frac{|\mathbf{c_g}|}{|\mathbf{k}|} - \frac{|\mathbf{c_p}|}{|\mathbf{k}|}.$$

Thus, wavepackets whose carrier wave has the wavenumber of a phase speed extremum have crests which move at the same speed as the wave envelope. This condition alone does not predict the existence of solitary waves. In fact, one can argue on physical grounds that in one dimension, solitary waves will exist generically if the phase speed has an extremum, but in two dimensions a *minimum* is required [14]. If these conditions are satisfied at $\mathbf{k} = \mathbf{0}$, one expects classical solitary waves, whereas at finite $\mathbf{k}$, one expects solitary wavepackets.

To understand the existence of a localized wave envelope, one can write an NLS equation from the Model by substituting the ansatz

$$\eta(x,y,t) = \epsilon A(\epsilon(x-ct), \epsilon y, \epsilon^2 t)e^{i\Theta} + \epsilon^2 A_2(x,y,t) + \epsilon^3 A_3(x,y,t) + * + \cdots . \tag{3.1}$$

The phase $\Theta = \mathbf{k_0}\cdot\mathbf{x} - \omega t$, where $\mathbf{k_0}$ is the carrier wave frequency, ω is the linear dispersion relation, and $*$ stands for complex conjugate. At $O(\epsilon^3)$ a solvability condition for A_3 is that the leading order envelope solves

$$iA_\tau + \lambda_1 A_{XX} + \lambda_2 A_{YY} = \chi |A|^2 A. \tag{3.2}$$

The variables in (3.2) in physical space are $X = \epsilon(x-ct), Y = \epsilon y$, and $\tau = \epsilon^2 t$. For the Model, at carrier wavenumber $\mathbf{k}_0 = (1,0)$, and for right-traveling waves with $c = \sqrt{2}$, the coefficients of (3.2) are

$$\lambda_1 = \frac{\sqrt{2}}{4}, \qquad \lambda_2 = \frac{\sqrt{2}}{2}, \qquad \text{and} \qquad \chi = -2\sqrt{2}.$$

Only the relative signs of λ_1, λ_2, and χ are meaningful, since the equation can be rescaled so that these coefficients all have magnitude one. The coefficients of the linear terms are directly related to the dispersion relation, $\lambda_1 = \frac{1}{2}\omega_{kk}(1,0)$ and $\lambda_2 = \frac{1}{2}\omega_{ll}(1,0)$. For $\lambda_1\chi < 0$, (3.2) is focusing in X and has line solitary wave solutions

$$A = \left|\frac{2}{\chi}\right|^{1/2} \operatorname{sech}\left(\frac{X}{\sqrt{\lambda_1}}\right) e^{i\tau}. \tag{3.3}$$

Of course if $\lambda_2\chi < 0$, then there are also line solitary waves which depend only on y. When, as is the case here, both products $\lambda_1\chi$ and $\lambda_2\chi$ are negative, the resulting equation is the elliptic or focusing 2D NLS equation which has fully localized lump solitary wave solutions. There is no closed form for the lump solutions to NLS, but they have been computed numerically [14, 17]. These localized solutions correspond to approximate envelopes of traveling wave solutions to the Model.

Line solitary waves, and fully localized, lump solitary waves have been computed to Euler [2, 5]. Here, we have computed such solutions for the Model. Example cross sections of line solitary waves are in Figure 1 and example lump solitary waves are in Figure 2. (Although many families of exotic solitary waves have been found in these types of problems, we follow the two principal families—that is, those with monotonically decaying envelopes—which, following the literature, we denote elevation and depression waves, respectively.) The speed-amplitude and speed-energy relations of depression line solitary waves in the Model are compared to those of Euler in Figure 3. The traveling wave solutions to the Euler equations were computed using a boundary integral formulation similar to that used in [2]. The speed-energy relations of lump solutions are given in section 4. Here, and throughout the paper, we have used the H_1 norm as a proxy for the energy since we do not have a closed form for the energy of the Model. It can be shown that the leading order term in the energy for Euler with surface tension is $||\eta||^2_{H_1}$ [20]. The details of the computational method used to find the lump solitary wave solutions are given in Appendix A.

4. Stability of solitary waves. The stability of wavepacket-type solitary waves has been studied in the 1D Euler problem and the 5th order KdV equation. In both, elevation waves are spectrally unstable and depression waves are spectrally stable [4, 10]. In a previous work, the authors presented simple one-way models for the 1D

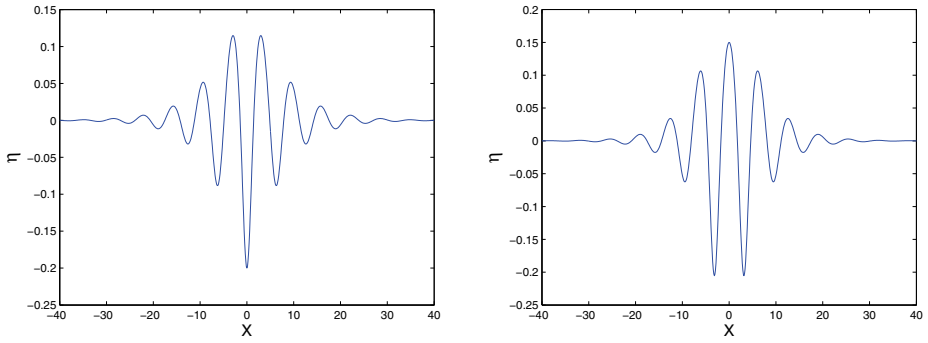

FIG. 1. *Example cross sections of depression (left) and elevation (right) line solitary wave solutions to the Model. Only a portion of the computational domain is shown.*

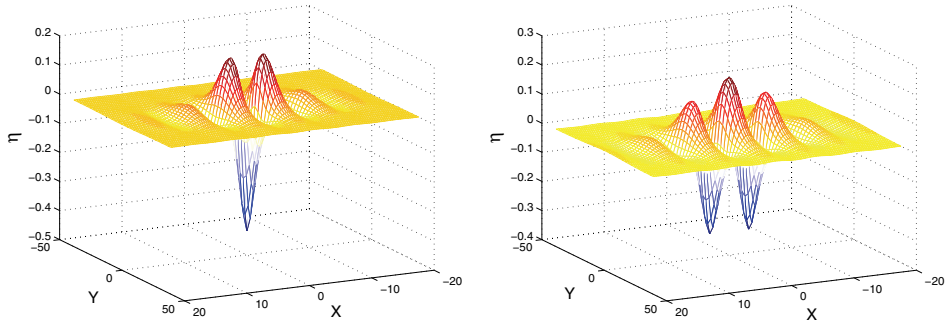

FIG. 2. *Examples of depression (left) and elevation (right) lump solitary wave solutions to the Model. Only a portion of the computational domain is shown.*

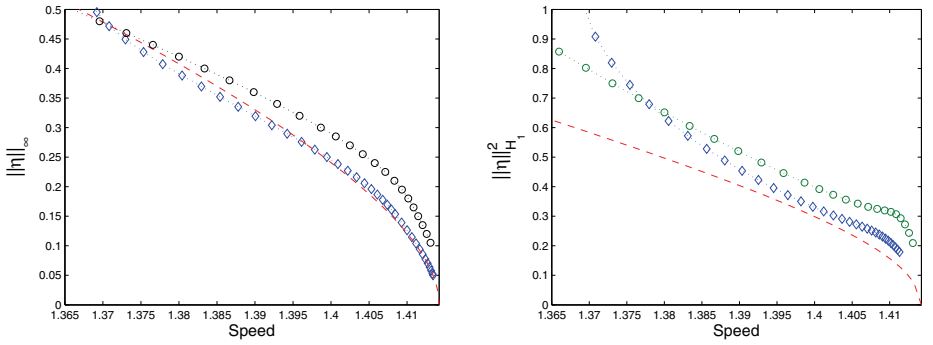

FIG. 3. *Left: The speed dependence of the infinity norm of depression solitary waves on a 1D free surface in the Model (diamonds) compared to waves in Euler (circles). Right: The H_1 norm of depression waves plotted as a function of the wave speed; diamonds are the Model, and circles are Euler. In both figures, the dashed curves are the approximations from the NLS equation, with coefficients from the Model, to second order given in section 4.*

deep water regime, where the stability results are similar [20]. (In one of the models, presented for contrast, depression waves change stability at finite amplitude, which is a consequence of a nonmonotonic speed-energy plot.) In this section we investigate the stability of both line and lump solitary waves of the Model.

The stability of line solitary waves to perturbations in the propagation direction (the 1D problem) follows the Euler result: elevation waves are unstable and depression waves are stable. This can be confirmed with both eigenvalue and time-dependent computations (not shown). These stability results are beyond the reach of the NLS equation, which does not differentiate between elevation and depression waves.

Consider then the stability of line solitary waves with respect to transverse perturbations. This is a classic problem: the KP equation was derived to study the stability of the KdV soliton with respect to transverse perturbations [25]. Since then this instability has been studied at length [26, 27]. In the context of gravity-capillary waves, wavepacket solitary waves of the 5th order KdV equation are unstable to transverse perturbations in the context of the corresponding KP equation [28], and line solitary waves are transversely unstable within the full Euler equations [29]. In [14] the authors also relate the transverse instability of a line wavepacket solitary wave to the transverse instability of its envelope within the NLS equation. Here we briefly present this argument applied to the Model.

The line solitary waves of the NLS equation (3.3) are unstable to transverse perturbations if the wavenumber of the perturbation $\kappa = (\kappa_{\mathbf{x}}, \kappa_{\mathbf{y}})$ is sufficiently small in the y direction, $0 < \kappa_y < \frac{\sqrt{3}}{|\lambda_2|}$ [30]. The line solitary waves in the NLS equation correspond to physical waves

$$\eta = 2\epsilon \left|\frac{2}{\chi}\right|^{1/2} \operatorname{sech}\left(\frac{\epsilon(x-\sqrt{2}t)}{\sqrt{|\lambda_1|}}\right)\cos(x-\sqrt{2}t) + O(\epsilon^2).$$

Recasting the stability condition in terms of the waves' height $||\eta||_\infty$ we find that the line solitary wave above is unstable for perturbations with wavelength

$$|k_y| < \left|\frac{3\chi}{8\lambda_2}\right|^{1/2} ||\eta||_\infty = \sqrt{\frac{3}{2}}||\eta||_\infty. \tag{4.1}$$

Equation (4.1) predicts that line solitary waves of arbitrary amplitude are unstable to sufficiently long perturbations. Depression line solitary waves of the Model have been evolved numerically, with a perturbation of $k_y = \frac{1}{8}$. Four different line solitary waves are compared: two on either side of the predicted threshold $||\eta||_\infty \approx 0.102$. The two waves below this threshold are stable, and the two waves above this threshold are unstable as shown in Figure 4.

Next, we consider the stability of fully localized lump solitary waves. Two families of lump solitary waves were computed (elevation and depression lumps), defined by the displacement from the mean level at the waves' center. We shall find that elevation lumps are unstable and that depression lumps are stable at small amplitude, unstable for a range of intermediate amplitudes, and then stable at larger amplitudes.

One type of instability of depression lumps can be understood by the dependence of the wave's energy on its speed. Perturbations of traveling waves have a neutral mode that arises from their Galilean invariance, and a change of stability of the system due to a bifurcation from this mode may arise only at local extrema of the speed-energy curve. This has been shown in Hamiltonian systems [31] and in a class of dispersive nonlinear equations [32]—of which the KdV equation [28] and KP equation [17] are

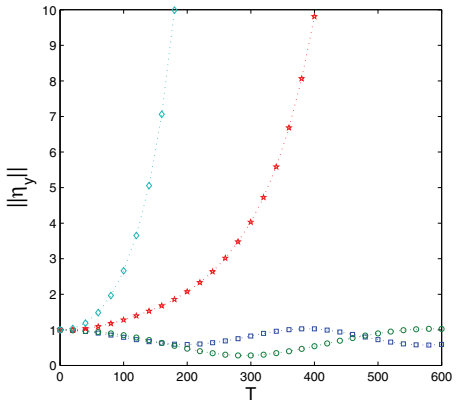

FIG. 4. *The evolution of* $||\eta_y||_2^2$, *normalized by its initial value, for four perturbed line solitary waves. In all cases the initial data is* $\eta = (1 + 0.1\cos(\frac{y}{8}))\bar{\eta}$, *where* $\bar{\eta}$ *is a line solitary wave. The diamonds, stars, circles, and squares correspond to* $||\bar{\eta}||_\infty$ *equaling* 0.15, 0.125, 0.1, *and* 0.075, *respectively. The predicted threshold for stability is* $||\bar{\eta}||_\infty = 0.102$.

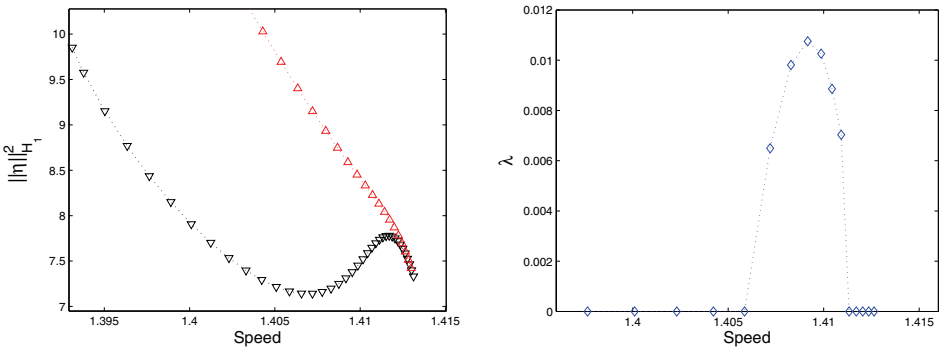

FIG. 5. *Left: The* H_1 *norm of elevation (triangles pointing up) and depression waves (triangles pointing down) plotted as a function of the waves speed. Right: The largest unstable eigenvalue of depression waves, estimated from the nonlinear evolution. The change of stability corresponds to the extrema of the energy.*

examples. Despite the fact that the Model does not belong to these classes, and that we do not have an explicit form for the energy, we conclude, numerically, that the stability of traveling lumps can still be understood via the graph of the wave speed versus its approximate energy (see Figure 5). The figure confirms an unstable eigenvalue in an interval approximately equal to the interval in which the approximate energy is increasing with speed.

The small amplitude limit of the speed energy relation can be obtained when the envelope of the solution to the truncated Euler equation is close to the localized solution to the NLS equation. The solutions are approximated by the series

$$\eta(x, y, t) = \epsilon A(\epsilon(x - ct), \epsilon y, \epsilon^2 t)e^{i\Theta} + \epsilon^2 D A^2 e^{2i\Theta} + * + \cdots, \tag{4.2}$$

where A solves (3.2) and $D = -2$. Substituting into the approximate energy $\int \eta_x^2 + \eta^2$,

and collecting terms gives asymptotic predictions for the wave energy:

$$\text{(4.3a)} \qquad \text{1D} \qquad \text{Energy} \sim \epsilon I_0 + \epsilon^3 I_1,$$

$$\text{(4.3b)} \qquad \text{2D} \qquad \text{Energy} \sim I_0 + \epsilon^2 I_1.$$

The coefficients are

$$I_0 = 4\frac{\Pi|\lambda_j|^{1/2}}{|\chi|}\int \rho^2\, dxdy, \qquad I_1 = \frac{\Pi|\lambda_j|^{1/2}}{|\chi|}\int \frac{10|D|^2}{|\chi|}\rho^4 + \frac{2}{|\lambda_1|}\rho_x^2 + \frac{2}{|\lambda_2|}\rho_y^2\, dxdy.$$

For 1D waves $\rho_y = 0$, the integrals are only in x, and the product $\Pi|\lambda_j|^{1/2} = |\lambda_1|^{1/2}$. The variable $\rho(x, y)$ satisfies the eigenvalue problem

$$\Delta\rho + \rho^3 = W\rho, \tag{4.4}$$

obtained by setting $A = \chi^{-1/2}\rho(|\lambda_1|^{-1/2}X, |\lambda_2|^{-1/2}Y)e^{iW\tau}$ and with the conditions that $\rho \to 0$ at infinity and $\rho(0, 0) = 1$. We define Δc as the difference between the solitary wave speed C and the linear bifurcation speed c; then $\Delta c = C - \sqrt{2} \sim -\epsilon^2 W$. For right-traveling waves, $\Delta c < 0$. The family of amplitude-dependent solutions results from the scaling invariance $\rho \to \mu\rho(\mu X, \mu Y)$, $W \to \mu^2 W$.

The NLS solitary wave solution can be used to determine W and the integrals of ρ for 1D waves. Using $\rho(x) = \operatorname{sech}(x/\sqrt{2})$ yields

$$W = 1/2, \quad \int \rho^2 = 2\sqrt{2}, \quad \int \rho^4 = 4\sqrt{2}/3, \quad \int \rho_x^2 = \sqrt{2}/3.$$

Numerically computed radially symmetric ground state solutions to (4.4) for the 2D problem give

$$W \approx 0.204, \quad \int \rho^2 \approx 11.70, \quad \int \rho^4 \approx 4.81, \quad \int \rho_x^2 = \int \rho_y^2 \approx 1.20.$$

For the Model, the energy predictions are

$$\text{(4.5)} \qquad \text{1D} \qquad \text{Energy} \sim 2^{5/4}|\Delta c|^{1/2} + \frac{2^{3/4}16}{3}|\Delta c|^{3/2},$$

$$\text{(4.6)} \qquad \text{2D} \qquad \text{Energy} \approx 8.27 + 67.8|\Delta c|.$$

Similarly, one can also get the speed-amplitude relation valid for both line and lump solitary waves

$$||\eta||_\infty \sim \left|\frac{4}{\chi W}\right|^{1/2}(\Delta c)^{1/2} + \left|\frac{2D}{\chi W}\right|\Delta c. \tag{4.7}$$

The 1D predictions are compared to the computations in Figure 3. In two dimensions the situation is very interesting: the waves have *finite* energy as the amplitude tends to zero. The value of this energy in our computation does not agree very well with the prediction (approximately 8.27 versus 7.25), probably due to domain truncation errors, which become important near bifurcation.

A further type of possible instability is the focusing instability, related to the phenomenon of wave collapse in the 2D focusing NLS equation. To understand this, consider the rescaled elliptic NLS equation, which reads

$$iA_\tau + A_{XX} + A_{YY} = -|A|^2 A, \tag{4.8}$$

with the two conserved quantities

$$M = \int |A|^2 dX dY \qquad \text{and} \qquad E = \int |\nabla A|^2 - \frac{1}{2}|A|^4 dX dY.$$

A well-known result is that localized solutions with $E < 0$ initially have a finite time singularity. The argument, due to Zakharov, considers the second derivative of the second moment of $|A|^2$:

$$\frac{d^2}{dt^2} M_2 = \frac{d^2}{dt^2} \int \int (X^2 + Y^2)|A|^2 dX dY = 8E. \tag{4.9}$$

Since E is a constant of motion, M_2 will become zero in finite time when $E < 0$. Since $M > 0$, this implies a concentration singularity at the origin. This singularity is known as wave collapse. On the other hand, if $E > 0$, we expect the M_2 to increase without bound, and therefore the wave disperses.

Localized lump solutions of (4.8) satisfy (4.4) with $A = \rho(X, Y)e^{iW\tau}$ and have $E = 0$ since M_2 is constant. In fact this can be used to prove that $W > 0$ since from (4.4) and $E = 0$

$$W = \frac{\int \rho^4 - \int (\nabla \rho)^2}{\int \rho^2} = \frac{\int \rho^4}{2 \int \rho^2}.$$

If we have a solution A with $E = 0$ (denoted $E[A] = 0$), then $E[(1 + \delta)A] < 0$ when $\delta > 0$ and $E[(1 + \delta)A] > 0$ when $-1 < \delta < 0$. Thus, for amplitude perturbations, the lump solitary waves lie at the boundary between wave collapse and dispersion.

The "ghost" of this property of the envelope equation appears in the primitive Model equation. To see this, we perturb the magnitude of a solitary wave $\tilde{\eta}$,

$$\eta = (1 + \delta)\tilde{\eta},$$

and then use η as initial data for numerical time evolution. We use a solitary wave $\tilde{\eta}$ which is stable according to the prediction of its speed-energy plot. The resulting evolution is dependent on both the sign and size of the perturbation, δ. For $\delta > 0$, when the NLS equation predicts wave collapse, the Model's waves grow initially and evolve to what appears to be a quasi-periodic oscillation about a stable wave at larger amplitude (slower speed). We do not see evidence of a singularity, and in the Lyapunov sense, the wave appears stable. For $\delta < 0$, when the NLS equation predicts that the wave disperses, there are two observed phenomena. For very small perturbations, the waves in the Model evolve to oscillate about a stable wave of smaller amplitude (faster speed) and thus again appear Lyapunov stable. For slightly larger perturbations, waves in the Model disperse into a radiated wave field, as predicted by the focusing NLS equation. The conclusion is that the focusing mechanism of the 2D NLS equation is at play, leading to transient growth, but that the waves chosen appear Lyapunov stable. The evolution of the wave magnitude for four perturbations is shown in Figure 6.

Lastly, we consider a possible instability due to resonant triads of waves. This instability is completely outside the NLS regimes as it involves waves "distant" in wavenumber space. We shall compute the triad equations for the resonant interactions of weakly nonlinear monochromatic waves in the Model, one of which has the wavenumber of the carrier wave for our solitary wave. The triad equations can be used

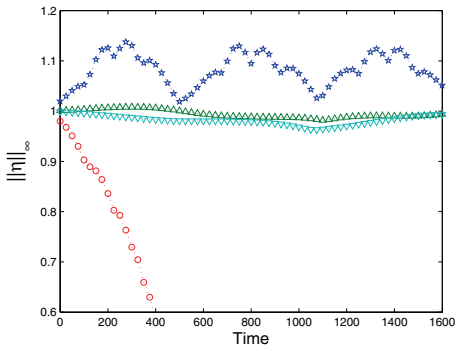

FIG. 6. *The evolution of* $||\eta||_\infty$*, normalized by its initial value, of a depression solitary wave with its magnitude perturbed,* $\eta = (1+\delta)\tilde{\eta}$*. For positive perturbation,* $\delta = 0.02$ *(stars), the wave oscillates about a larger (slower) depression wave. For negative perturbation,* $\delta = -0.02$ *(circles), the wave disperses into a radiated wave field. For smaller perturbations, here* $\delta = 0.001$ *(triangles pointing up) and* $\delta = -0.001$ *(triangles pointing down), the wave oscillates about a slightly slower (or faster, respectively) wave of approximately the same amplitude. The unperturbed wave in all cases has* $||\eta||_\infty = 0.3305$.

to understand the primary nonlinear interactions at quadratic order [33]. Consider the ansatz

(4.10)
$$\eta = \epsilon A_1(\epsilon t)e^{i\mathbf{k_1}\cdot\mathbf{x}-i\omega_1 t} + \epsilon A_2(\epsilon t)e^{i\mathbf{k_2}\cdot\mathbf{x}-i\omega_2 t} + \epsilon A_3(\epsilon t)e^{i\mathbf{k_3}\cdot\mathbf{x}-i\omega_3 t} + * + \epsilon^2 B(\mathbf{x},t) + \cdots,$$

where $*$ refers to the complex conjugate and $\omega_i = \sqrt{|\mathbf{k_i}| + |\mathbf{k_i}|^3}$. At $O(\epsilon^2)$ a solvability condition for $B(\mathbf{x},t)$ is that the A_i solve the triad equations

$$-2i\omega_1 A_{1,T} + C(-\mathbf{k_2},\mathbf{k_3})\bar{A}_2 A_3 = 0, \tag{4.11a}$$

$$-2i\omega_2 A_{2,T} + C(-\mathbf{k_1},\mathbf{k_3})\bar{A}_1 A_3 = 0, \tag{4.11b}$$

$$-2i\omega_3 A_{3,T} + C(\mathbf{k_1},\mathbf{k_2})A_1 A_2 = 0 \tag{4.11c}$$

whenever

$$\mathbf{k_1} + \mathbf{k_2} = \mathbf{k_3} \quad \text{and} \quad \omega_1 + \omega_2 = \omega_3,$$

with $C(\mathbf{k_i},\mathbf{k_j})$ being the triad interaction coefficients obtained in a straightforward way from the Model.

Given that the solitary waves solutions to the Model are supported near wavenumber $\mathbf{k} = (1,0)$, it is natural to examine the predictions of the triad equations for a set of waves including this one. We consider triads of the form $\mathbf{k_1} = (1,0)$, $\mathbf{k_2} = (\alpha,\beta)$, $\mathbf{k_3} = (1+\alpha,\beta)$. There is a one parameter family of such triads, including the simplest case $\beta = 0$ with $\alpha \approx 0.4951$. We use (4.11) to study the stability of A_1 with respect to perturbations in the other two waves in the triad by linearizing about $A_1 = 1$, $A_2 = 0$, $A_3 = 0$ [33], setting

$$A_1 = 1 + \mu\tilde{A}_1, \quad A_2 = \mu\tilde{A}_2, \quad \text{and} \quad A_3 = \mu\tilde{A}_3$$

(for μ small) and neglecting quadratic terms in μ. This leads to the "pump-wave" approximation for, say, $\tilde{A}_2$,

$$\tilde{A}_{2,tt} + \frac{C(-\mathbf{k_1},\mathbf{k_3})C(\mathbf{k_1},\mathbf{k_2})}{4\omega_2\omega_3}\tilde{A}_2 = 0.$$

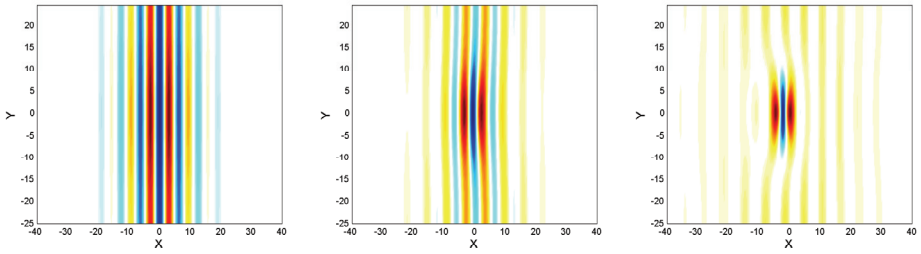

FIG. 7. *The evolution of a line solitary wave into a lump solitary wave and some radiation, viewed from above. From left to right* $t = 0$, 170, *and* 300.

From this equation we can conclude that the solution $A_1 = 1$ is stable in the triad equations (4.11) when the product $C(-k_1, k_3)C(k_1, k_2) > 0$. This can be shown numerically from the interaction coefficients for the full one parameter family of possible triads in our system (and is related to the fact that in Hamiltonian systems, A_1 is stable in any triad with $|\mathbf{k_2}| < |\mathbf{k_1}| < |\mathbf{k_3}|$).

5. Dynamics of solitary waves. In this section we present some dynamics of solitary wave solutions to the Model. It is evolved numerically using a pseudospectral method in space, and 4th order Runge–Kutta in time, as in [34]. Typical numbers of Fourier modes in (x, y) used in the time-dependent computations are 512×128. Three types of initial value problems are considered. First, line solitary waves with a small transverse perturbation are evolved. Second, unstable lump solitary waves are evolved. Finally, stable lumps are collided.

In section 4, a range of unstable transverse wavenumbers for line solitary waves of a particular amplitude was derived. This threshold was explored numerically and shown to agree well with numerical results. Here we observe how this linear instability manifests itself in the nonlinear wave evolution. The result is that, for small to moderate amplitudes, unstable line solitary waves evolve into depression lump solitary waves through a focusing mechanism. Snapshots of one evolution of a depression line solitary wave into a depression lump are shown in Figure 7. For larger amplitudes ($||\eta||_\infty \approx 0.3$) we observed cases in which there was evidence that the focusing mechanism resulted in wave-breaking, that is, $\eta_x \to \infty$. Of course, such phenomena is outside the realm of validity of the Model.

The stability of lump solitary waves was predicted using connections to the speed-energy plot; see Figure 5. From this prediction, we expect all elevation lumps to have the same stability properties; i.e., that they are unstable, as are their analogues in 1D and other model equations, but that depression lumps change stability at the local energy extrema as predicted by the growth rates. Thus we expect there to be a band of unstable depression waves at intermediate amplitudes. These predictions were confirmed numerically, but the nature of the nonlinear evolution of the unstable waves is different. Elevation waves are unstable and evolve into depression waves, whereas unstable depression waves radiate into linear waves. An example of an unstable elevation wave evolving into a depression wave is shown in Figure 8. An example of the unstable evolution of an intermediate amplitude depression wave is shown in Figure 9.

In addition to considering the dynamics of unstable lump solitary waves, we also consider the collisions of stable depression lumps. Three collision experiments are

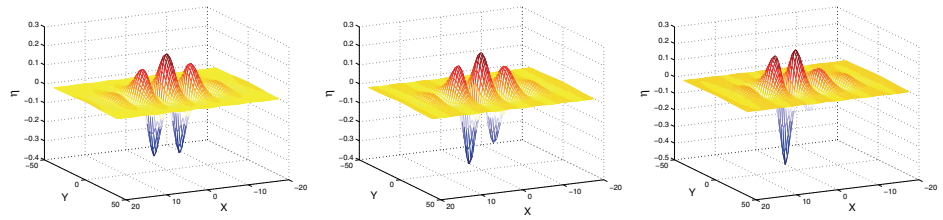

FIG. 8. *An unstable elevation wave at times $t = 0$ (left), $t = 425$ (center), and $t = 475$ (right). The deepest trough left of the centerline becomes a depression wave; the deepest trough right of the centerline dissolves into radiated waves. The computation is shown in a frame moving with the speed of the original wave, which moves to the right.*

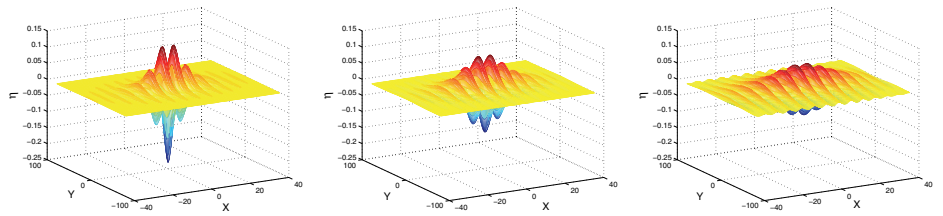

FIG. 9. *Snapshots of the evolution of an unstable depression wave in the Model. From left to right: $t = 0$, 2250, and 2650. The computation is shown in a frame moving with the speed of the original wave.*

presented. In the simplest collision, the waves move in opposite directions, toward each other, with their centers aligned. We refer to these as head-on collisions, and there appears to be no visible interaction between the waves. An example of a head-on collision is shown in Figure 10. In a second collision experiment, both waves move in the same direction with their centers aligned. The smaller (faster) wave overtakes the larger (slower) wave. We refer to this interaction as an overtaking collision. Overtaking collisions exhibit significant nonlinear interaction and result in a lone solitary wave, which is larger than both of the waves which collided to form it, and a radiated wave field. Snapshots of an overtaking collision are shown in Figure 11. The last experiment here is an overtaking collision, where the wave centers are not aligned. The goal of this experiment is to observe interactions which are not as weak as head-on collisions, yet not as strong as overtaking collisions with the centers aligned. If the offset is very small, offset overtaking collisions are identical to overtaking collisions. Similarly, for a very large offset, the interaction is very small and appears to be elastic, as in head-on collisions. For moderate displacements, we observe a qualitatively different behavior: two waves which interact to form two new waves of different sizes, moving at different speeds from those which formed them. In this interaction, little or no waves are radiated from the interaction. An example of such an offset collision is shown in Figure 12.

6. Conclusion. We present a quadratic truncation of Euler's equations for potential flow as a new model for solitary gravity-capillary waves in deep water. This model is isotropic and thus differs from the unidirectional and weakly 2D model introduced in [14] in much the same way as 2D Boussinesq equations (also called the Benney–Luke equations) differ from the Kadomtsev–Petviashvili equation in shallow water.

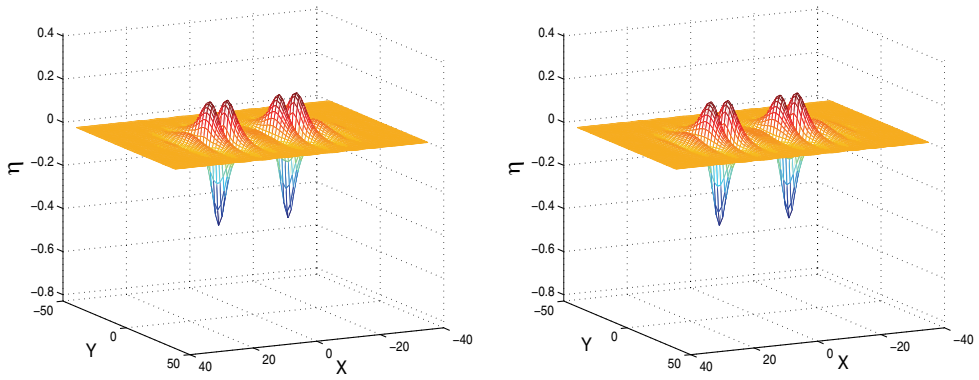

(a) T = 0

(b) T = 6.5

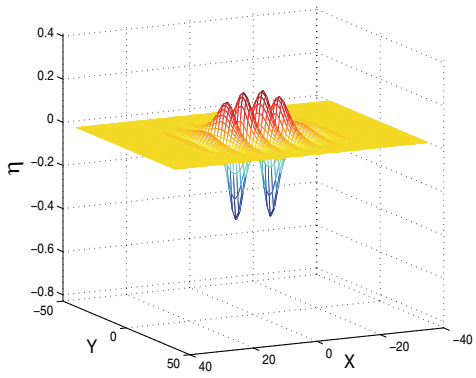

(c) T = 10.4

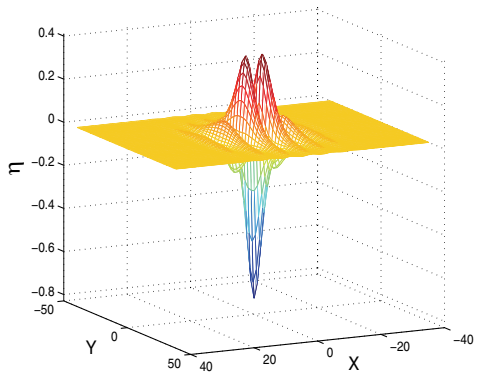

(d) T = 14.3

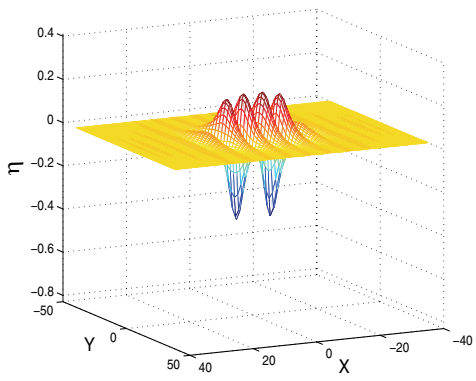

(e) T = 18.2

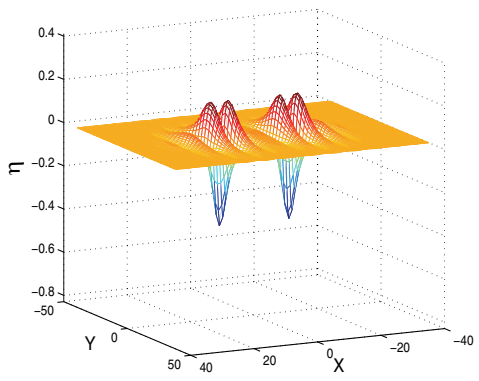

(f) T = 22.1

FIG. 10. *A head-on collision of solitary waves in the Model. The collision is shown in a stationary frame. Such a collision is outside the scope of the unidirectional model in* [14].

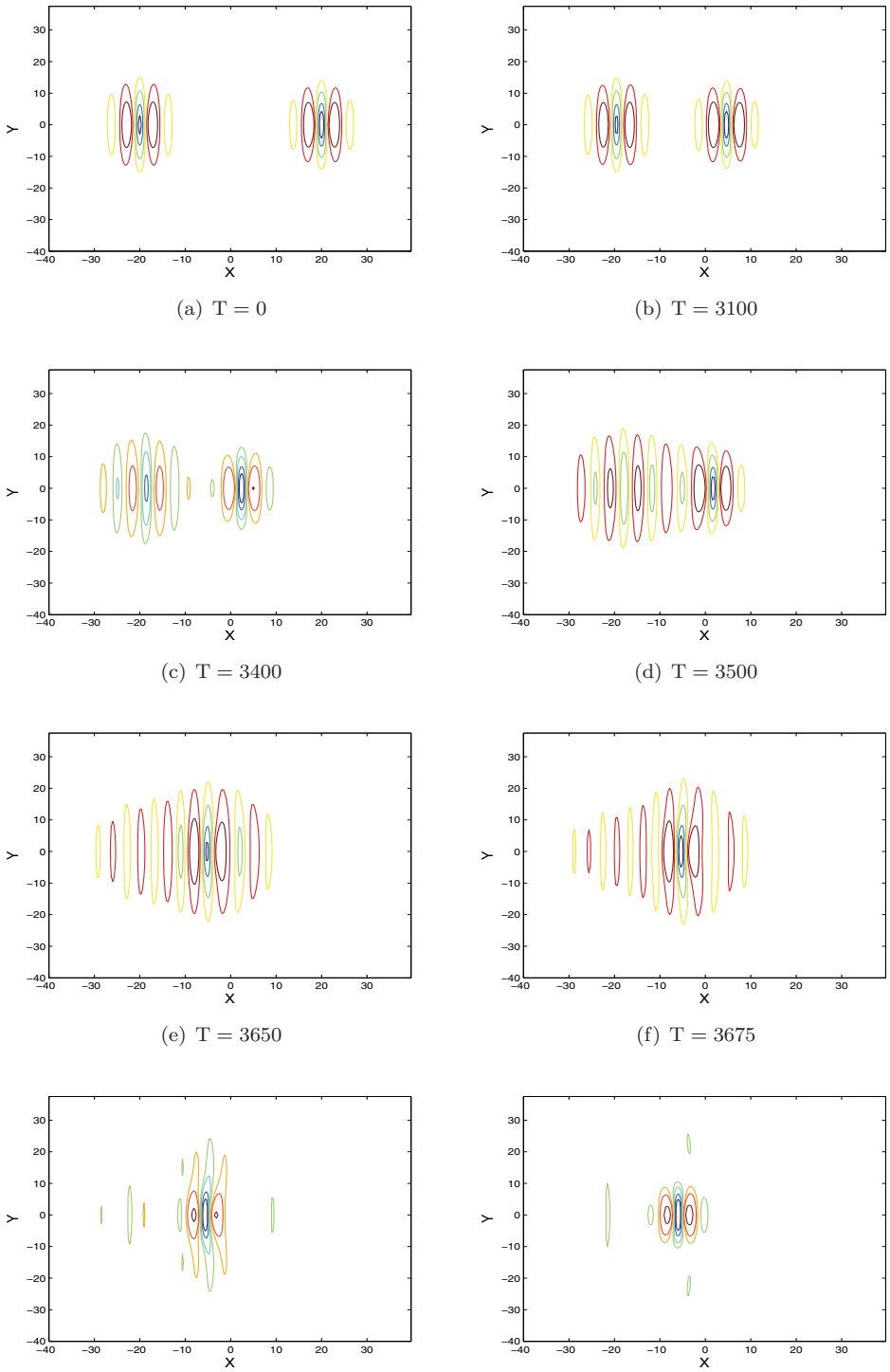

(a) T = 0 (b) T = 3100

(c) T = 3400 (d) T = 3500

(e) T = 3650 (f) T = 3675

(g) T = 3700 (h) T = 3750

FIG. 11. *Snapshots of an overtaking collision of two depression lump solitary waves, where the wave centers are aligned in the Model. The images are shown in a frame moving to the left at speed equal to that of the larger and slower wave, which is on the left in (a). After the collision, a lone solitary wave, larger than both of the original waves, remains. Some waves are radiated during the interaction.*

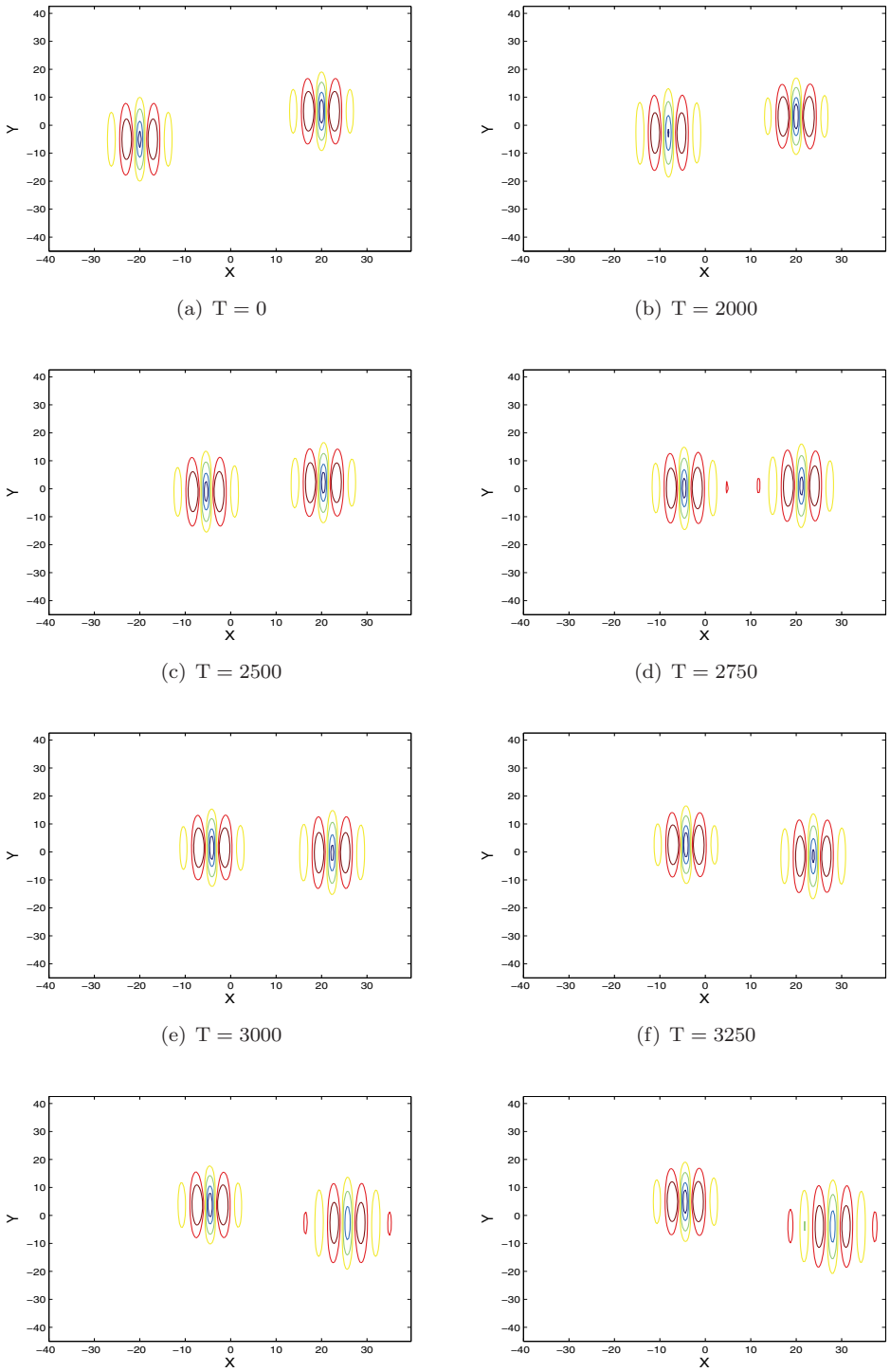

(a) T = 0 (b) T = 2000

(c) T = 2500 (d) T = 2750

(e) T = 3000 (f) T = 3250

(g) T = 3500 (h) T = 3750

FIG. 12. *Snapshots of an overtaking collision of two depression lump solitary waves, where the wave centers are offset by* 10 *space units in the Model. The images are shown in a frame moving to the right at speed equal to that of the larger and slower wave, which is on the right in (a). After the interaction, two waves remain, but they have different amplitudes, speeds, and propagation direction than the original waves.*

We study in detail two branches of solitary wave solutions on both a 1D free surface and a 2D free surface. These waves are called elevation and depression waves, based on their central displacement from the mean level. The waves on the 1D free surface have the same stability as their Euler counterparts. These waves can be extended trivially as line solitary waves on a 2D free surface. The waves' envelopes are approximated by line solitary wave solutions of the focusing NLS equation. Line solitary waves are unstable to transverse perturbations, at a threshold predicted by the NLS equation. The stability of lump solitary waves on a 2D surface is considered, both via the speed energy plot and by numerical time evolution. We find that elevation lumps are unstable and the stability of depression lumps depends on the wave amplitude. The unstable band occurs between two extrema in the speed-energy plot. The dynamics of unstable waves are also investigated. Unstable elevation waves evolve into depression waves and radiated wave fields. Unstable depression waves decay into a radiated wave field. Other possible instabilities are considered: the wave collapse predictions of the NLS equation for the wave envelope are compared to dynamics of waves in the physical equation, and triad instabilities are ruled out. Three collisions of lump solitary waves are presented, capturing a broad range of behaviors. Interactions are presented where two waves collide almost elastically, where two waves form one wave, and where two waves form two waves, different from the original ones. In the latter two cases a noticeable radiated wave field is present We find it remarkable that, in spite of all the solitary waves we consider being subject to the wave collapse or dispersion mechanism of the focusing NLS equation, they form robust solutions in the time-dependent evolution.

Appendix. Computing solitary waves. In this appendix we discuss the computation of solitary wave solutions to the model equation. The Model has two classes of solitary waves on a 2D free surface: those that decay only in the propagation direction (line solitary waves) and those that decay in both directions (lump solitary waves). Line solitary waves are the trivial 2D extension of solitary waves on a 1D free surface, constant in the transverse direction. Line solitary waves are computed in the 1D version of the Model using Newton's method on the Fourier coefficients, as in [20, 13]. The NLS wavepacket is used for an initial guess, $\eta \sim \epsilon \mathrm{sech}(\epsilon x)\cos(x)$.

To compute lump solitary waves, we use a more sophisticated continuation procedure. First, traveling solutions to the Model are expanded in Fourier components:

$$\eta(x,t) = \sum_m \sum_n a_{n,m} e^{ik_n(x-ct)+ik_m y}.$$

The equation is projected onto M Fourier modes in x and N Fourier modes in y, yielding a nonlinear system of NM algebraic equations for $NM+1$ unknowns: the NM Fourier amplitudes and the speed c. We add to this an equation fixing a measure of the solution amplitude (either a norm or the height at the central crest). Solutions for different amplitudes are computed by continuation. It is, however, difficult to find an appropriate initial guess for the solutions (focusing NLS lumps do not appear to give good results). Thus we use an algorithm similar to that used in [5, 2]. The idea is to add an artificial forcing to the Model:

$$\eta_{tt} + \Omega^2 \eta + N(\eta, \eta_t) = \delta F(x - ct, y). \tag{A.1}$$

The forcing function used here is

$$F(x-ct,y) = \frac{d^2}{dt^2}\left(e^{-0.15(x-ct)^2 - 0.01y^2}\right).$$

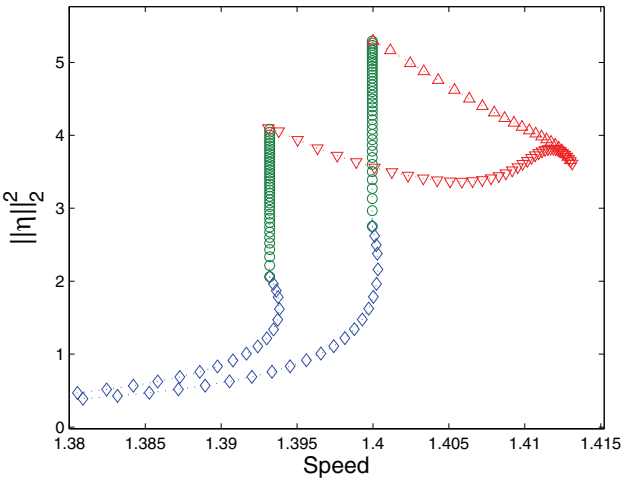

FIG. 13. *The continuation diagram for the Model. Diamonds mark the forced branches (ϵ fixed, $||\eta||_\infty$ increasing); circles mark the branches where ϵ decreases to zero; triangles mark the unforced branches ($\epsilon = 0$; triangles pointing up are elevation waves; triangles pointing down are depression waves).*

Newton's method is used to find solutions to (A.1) with small forcing (a typical value of δ is 0.1) using $\eta = 0$ as an initial guess. The computed solution is a small perturbation of the linear solution to the forced problem, which moves at the speed of the forcing. Continuation is used to compute a forced branch of solutions of increasing amplitude with fixed amplitude forcing, allowing the speed to vary. In the large amplitude range of this branch, the forcing becomes small relative to the nonlinearity. Once this is the case, we can decrease the amplitude of the forcing δ up to a solution to the unforced Model. The resulting solution is used to find continuous families of these waves, again via continuation. A diagram showing this continuation procedure is presented in Figure 13. The typical numbers of modes used in the forced branches of the continuation process are $N = 128$, $M = 32$. Once unforced solutions are found, these numbers are increased to $N = 256$ and $M = 64$.

Acknowledgment. The authors thank the National Science Foundation for its support. The second author also wishes to thank the École Normale Supérieure de Cachan for sponsoring his visit there during the course of this research.

REFERENCES

[1] M. S. LONGUET-HIGGINS, *Capillary gravity waves of the solitary type on deep water*, J. Fluid Mech., 200 (1989), pp. 451–478.
[2] J.-M. VANDEN-BROECK AND F. DIAS, *Gravity-capillary solitary waves in water of infinite depth and related free surface flows*, J. Fluid Mech., 240 (1992), pp. 549–557.
[3] M. S. LONGUET-HIGGINS, *Capillary gravity waves of the solitary type and envelope solitons on deep water*, J. Fluid Mech., 252 (1993), pp. 703–711.
[4] D. C. CALVO, T. S. YANG, AND T. R. AKYLAS, *Stability of steep gravity-capillary waves in deep water*, J. Fluid Mech., 452 (2002), pp. 123–143.
[5] E. I. PARAU, J.-M. VANDEN-BROECK, AND M. J. COOKER, *Nonlinear three-dimensional gravity-capillary solitary waves*, J. Fluid Mech., 536 (2005), pp. 99–105.
[6] T. B. BENJAMIN, *A new kind of solitary wave*, J. Fluid Mech., 245 (1992), pp. 401–411.

[7] T. R. Akylas, *Envelope solitons with stationary crests*, Phys. Fluids A, 5 (1993), pp. 789–791.
[8] G. Iooss and P. Kirrmann, *Capillary gravity waves on the free surface of an inviscid fluid of infinite depth. Existence of solitary waves*, Arch. Rational Mech. Anal., 136 (1996), pp. 1–19.
[9] M. D. Groves and S.-M. Sun, *Fully localized solitary-wave solutions of the three-dimensional gravity-capillary water-wave problem*, Arch. Rational Mech. Anal., 188 (2008), pp. 1–91.
[10] D. C. Calvo, T. S. Yang, and T. Akylas, *On the stability of solitary waves with decaying oscillatory tails*, R. Soc. Lond. Proc. Ser. A Math. Phys. Eng. Sci., 456 (2000), pp. 469–487.
[11] B. Malomed and J.-M. Vanden-Broeck, *Solitary wave interactions for the fifth-order KdV equation*, in Mathematical Problems in the Theory of Water Waves (Luminy, 1995), Contemp. Math. 200, AMS, Providence, RI, 1996, pp. 133–143.
[12] P. A. Milewski and J.-M. Vanden-Broeck, *Time-dependent gravity-capillary flows past an obstacle*, Wave Motion, 29 (1999), pp. 63–79.
[13] K. M. Berger and P. A. Milewski, *The generation and evolution of lump solitary waves in surface-tension-dominated flows*, SIAM J. Appl. Math., 61 (2000), pp. 731–750.
[14] B. Akers and P. A. Milewski, *A model equation for wavepacket solitary waves arising from capillary-gravity flows*, Stud. Appl. Math., 122 (2009), pp. 249–274.
[15] B. Kim and T. R. Akylas, *On gravity-capillary lumps*, J. Fluid Mech., 540 (2005), pp. 337–351.
[16] B. Kim and T. R. Akylas, *On gravity-capillary lumps. Part* 2: *Two-dimensional Benjamin equation*, J. Fluid Mech., 557 (2006), pp. 237–256.
[17] T. R. Akylas and Y. Cho, *On the stability of lumps and wave collapse in water waves*, Phil. Trans. R. Soc. A, 366 (2008), pp. 2761–2774.
[18] M. S. Longuet-Higgins and X. Zhang, *Experiments on capillary gravity waves of the solitary type on deep water*, Phys. Fluids, 9 (1997), pp. 1963–1968.
[19] J. Diorio, Y. Cho, J. H. Duncan, and T. R. Akylas, *Gravity-capillary lumps generated by a moving pressure source*, Phys. Rev. Lett., 103 (2009), article 214502.
[20] B. Akers and P. A. Milewski, *Model equations for gravity-capillary waves in deep water*, Stud. Appl. Math., 121 (2008), pp. 49–69.
[21] N. B. Vargraftik, B. N. Volkov, and L. D. Voljak, *International tables of the surface tension of water*, J. Phys. Chem. Ref. Data, 12 (1983), pp. 817–820.
[22] P. A. Milewski, *Fast communication: Three-dimensional localized gravity-capillary waves*, Comm. Math. Sci., 3 (2005), pp. 89–99.
[23] M. Chen, J. L. Bona, and J. C. Saut, *Boussinesq equations and other systems for small-amplitude long waves in nonlinear dispersive media.* I: *Derivation and linear theory*, J. Nonlinear Sci., 12 (2002), pp. 283–318.
[24] T.-S. Yang and T. R. Akylas, *On asymmetric gravity-capillary solitary waves*, J. Fluid Mech., 330 (1997), pp. 215–232.
[25] B. B. Kadomtsev and V. Petviashvili, *On the stability of solitary waves in weakly dispersing media*, Soviet Phys. Dokl., 15 (1970), pp. 539–541.
[26] T. J. Bridges, *Transverse instability of solitary wave states in the water-wave problem*, J. Fluid Mech., 439 (2001), pp. 255–278.
[27] J. C. Alexander, R. L. Pego, and R. L. Sachs, *On the transverse instability of solitary waves in the Kadomtsev-Petviashvilli equation*, Phys. Lett. A, 226 (1997), pp. 187–192.
[28] D. E. Pelinovsky and R. H. J. Grimshaw, *Asymptotic methods in soliton stability theory*, Nonlinear Instability Anal., 12 (1997), pp. 245–312.
[29] B. Kim and T. R. Akylas, *Transverse instability of gravity-capillary solitary waves*, J. Engrg. Math., 58 (2007), pp. 167–175.
[30] K. Rypdal and J. J. Rasmussen, *Stability of solitary structures in the nonlinear Schrödinger equation*, Physica Scripta, 40 (1988), pp. 192–201.
[31] P. G. Saffman, *The superharmonic instability of finite amplitude water waves*, J. Fluid Mech., 159 (1985), pp. 169–174.
[32] B. Akers and P. A. Milewski, *A stability result for solitary waves in nonlinear dispersive equations*, Commun. Math. Sci., 6 (2008), pp. 791–797.
[33] A. D. D. Craik, *Wave Interactions and Fluid Flows*, Cambridge University Press, Cambridge, UK, 1985.
[34] P. A. Milewski and E. G. Tabak, *A pseudospectral procedure for the solution of nonlinear wave equations with examples from free-surface flows*, SIAM J. Sci. Comput., 21 (1999), pp. 1102–1114.